Proceedings of the 25th International Conference on
Port and Ocean Engineering under Arctic Conditions
June 9-13, 2019, Delft, The Netherlands

Peridynamic Simulations on Propeller-Ice Impact

Liyu Ye[1], Chunyu Guo[1], Chao Wang[1], Chunhui Wang[1]
[1] College of Shipbuilding Engineering, Harbin Engineering University, Heilongjiang Province 150001, PR China

ABSTRACT

When the ice-going ship navigates in the ice rubble condition, small ice pieces will continue to impact with propeller blades. Due to the high rotational speed of propeller blades, extreme contact forces may dominate the loading on the propeller blade, which may cause large deformation and damage of blades. The complexity of propeller-ice impact process adds challenges to establish a reliable numerical model. In this paper, a numerical method based on peridynamics has been introduced to simulate propeller-ice impact. The ice is discretized into a number of particles, and the ice failure process during impact is simulated by peridynamics. The continuous contact detection algorithm is developed to detect the contact between the propeller surface and ice particles and calculate the ice loads. Based on the numerical model, we study the characteristics of ice failure and dynamic load. The effects of ice shape and velocity on the results are analyzed. It is concluded that the numerical model can capture the formation of cracks and ice pieces during propeller-ice impact vividly. The results are helpful to understand the mechanism of propeller-ice impact.

KEY WORDS: Propeller-ice impact; Ice failure; Ice load; Peridynamics, Contact detection.

INSTRUCTION

The Arctic region has become a hot spot for international competition and cooperation. Many countries pay more and more attention to polar research and exploitation. Ice-going ship is an indispensable means for countries to implement polar strategies. When the ice-going ship navigates in the ice rubble condition, small ice pieces will continue to impact on the propeller. Due to the high rotational speed of the propeller, extreme contact forces may dominate the loading on the propeller blade, which will cause large deformation and damage of blades. Therefore, the study of propeller-ice impact problem is a key part of the ice-class propeller design.

Propeller-ice impacts have been researched by theoretical analysis and experimental investigation. In the theoretical analysis, Wind (1983) developed a propeller-ice impact model and the contact loads were calculated by linear momentum theory, but the model assumed that the ice piece impacted with the blade back and didn't consider the rotation of the propeller. Laskow et al (1985) derived the calculation formula for the impact ice on duct propeller and open propeller. Kannari (1994) developed a propeller-ice impact model with assuming that forward blade force is caused by propeller-ice impact, and the relative velocity

between propeller and ice is obtained by rotational velocity of propeller and ship velocity. In experiment investigation, Brouwer (2013) designed a model test setup, which is capable of measuring the impact of ice on a propeller by means of measuring the highly dynamic forces and moments in all directions during propeller-ice impact. From the literature reviews, it can be seen that more attention has been paid to theoretical analysis and model experiment, but the numerical method is limited. Since the implementation of propeller-ice contact experiment is very difficult, many actual operational conditions cannot be carried out. A lot of mechanics for propeller-ice contact haven't been revealed. The numerical method can overcome these shortcomings and simulate the situations that model experiment could not do.

Due to the complex physical and mechanical properties of ice and freedom motion of ice pieces, it is difficult to research on propeller-ice impacts with the numerical method. Over the past few decades, the mesh method and meshless method have been used to simulate ice failure problem. Mesh method is mainly by the Finite element method. However the Finite Element Method is based on continuum mechanics, it is difficult in dealing with the fracture and damage mechanics of ice. For meshless method, a variety of numerical solution methods have been developed, such as smoothed particle hydrodynamic (SPH) (Shen. 2000), Distinct Element Method (DEM) (Lau et al. 2010), Peridynamic method (PD) and so on.

It is advisable to use a proper numerical method to simulate ice failure problem. The peridynamic method, proposed firstly by Silling (2000), is suitable for modeling the fracture problems. Ye et al (2017) developed propeller-ice contact model by combining the peridynamic method and continuous contact detection algorithm. Wang et al. (2018) investigated the propeller-ice contact and milling loads under different conditions based on the PD method, and the ice failure patterns and the changing regularity of the milling loads for the blade were obtained. In this paper, peridynamics is applied to study the propeller-ice impacts. First, the basic bond-based peridynamics theory is introduced. Then, the numerical model of propeller-ice impact has been established, and the contact detection method and calculation formula of contact ice load have been introduced. Last, numerical simulations are conducted to study the characteristics of ice failure and dynamic load. The effect of ice shape and velocity on the results is been discussed.

BOND-BASED PERIDYNAMIC THEORY

Peridynamics is a nonlocal continuum solid mechanics method, and its equations of motion are defined in integral form rather than conventional partial differential commonly used in the finite element method. The peridynamic equation of motion, for any particles of position $\boldsymbol{x}$ and time t at a reference configuration, can be expressed as follow:

$$\rho\ddot{\boldsymbol{u}}(\boldsymbol{x},t)=\int_{H_x}\boldsymbol{f}\left(\boldsymbol{u}(\boldsymbol{x}',t)-\boldsymbol{u}(\boldsymbol{x},t),\boldsymbol{x}'-\boldsymbol{x}\right)\mathrm{d}V_{x'}+\boldsymbol{b}(\boldsymbol{x},t) \tag{1}$$

where H_x is the domain of integration within the horizon of the material particle $\boldsymbol{x}$, $\boldsymbol{u}$ is the displacement vector of the material particle $\boldsymbol{x}$, ρ is mass density. The vector $\boldsymbol{f}$ is a pairwise force density function defined as the force per unit volume that the material particle at $\boldsymbol{x}'$ exerts on the material particle at $\boldsymbol{x}$. The peridynamic equation of motion is formulated by spatial integral equations which permit the peridynamic formulation to be effective everywhere.

To facilitating the presentation below, the relative position of two interacting particles is denoted by $\boldsymbol{\xi}=\boldsymbol{x}'-\boldsymbol{x}$ and its relative displacement is denoted by $\boldsymbol{\eta}=\boldsymbol{u}(\boldsymbol{x}',t)-\boldsymbol{u}(\boldsymbol{x},t)$, so the vector $\boldsymbol{\xi}+\boldsymbol{\eta}$ is the relative position of the two interacting particles at t. Thus, the pairwise force density function can be described as $\boldsymbol{f}(\boldsymbol{\eta},\boldsymbol{\xi})$, and its value depends on $\boldsymbol{\xi}$ and $\boldsymbol{\eta}$. Similar to the molecular dynamics, the material particles interacting with each other is called "bonds", which can be considered as a spring in the case of elastic interaction. The concept of a bond

that extends over a finite distance is a fundamental difference between the peridynamic theory and the classical theory.

In this peridynamic theory, there exists a positive number δ, called the horizon H_x. Beyond H_x the influence of the material particles interacting with $\boldsymbol{x}$ is assumed to vanish, such that

$$|\boldsymbol{\xi}| > \delta \Rightarrow \boldsymbol{f}(\boldsymbol{\eta}, \boldsymbol{\xi}) = 0 \quad \forall \boldsymbol{\eta}, \boldsymbol{\xi} \tag{2}$$

For a continuum, the pairwise forces are regarded as interactions between pairs of material particles, and the pairwise force density function must obey the linear and angular admissibility conditions, ensuring that the function does not violate Newton's third law of motion, which are shown as follows:

$$\boldsymbol{f}(-\boldsymbol{\eta}, -\boldsymbol{\xi}) = -\boldsymbol{f}(\boldsymbol{\eta}, \boldsymbol{\xi}) \quad \forall \boldsymbol{\eta}, \boldsymbol{\xi} \tag{3}$$

Eq. (3) assures conservation of linear momentum, and

$$(\boldsymbol{\xi} + \boldsymbol{\eta}) \times \boldsymbol{f}(\boldsymbol{\eta}, \boldsymbol{\xi}) = 0 \quad \forall \boldsymbol{\eta}, \boldsymbol{\xi} \tag{4}$$

Eq. 4 assures conservation of angular momentum, which means that the force vector between the material particles is parallel to their current relative position vector. For the micro-elastic material, Silling and Askari (2005) derived the pairwise force density function as:

$$\boldsymbol{f}(\boldsymbol{\eta}, \boldsymbol{\xi}) = \frac{\boldsymbol{\xi} + \boldsymbol{\eta}}{|\boldsymbol{\xi} + \boldsymbol{\eta}|} f\left(|\boldsymbol{\xi} + \boldsymbol{\eta}|, \boldsymbol{\xi}\right) \quad \forall \boldsymbol{\xi}, \boldsymbol{\eta} \tag{5}$$

where f is scalar bond force. Eq. (1) and Eq. (5) together constitute the totality of the peridynamic model for a nonlinear micro-elastic material, and a concept of failure is involved in this model. It can be assumed that the scalar bond force f depends only on bond stretch or bond strain s defined by

$$s = \frac{|\boldsymbol{\xi} + \boldsymbol{\eta}| - |\boldsymbol{\xi}|}{|\boldsymbol{\xi}|} = \frac{y - |\boldsymbol{\xi}|}{|\boldsymbol{\xi}|} \tag{6}$$

When the bond is intensional, the value of s is positive. Because there is no dependence of f on the direction of $\boldsymbol{\xi}$, such material is isotropic.

By making bonds to fail when they are deformed beyond a predetermined value, the simplest way to define failure into a constitutive model is established. Once a bond fails, it is failed forever, so the model is history dependent. Considering the prototype micro-elastic brittle (PMB) material, the bond force can be expressed as follows:

$$f(y(t), \boldsymbol{\xi}) = g(s(t, \boldsymbol{\xi}))\mu(t, \boldsymbol{\xi}) \tag{7}$$

where g is the linear scalar valued function defined by the following formula:

$$g(s) = cs \quad \forall s \tag{8}$$

where c is a constant. For linear elastic isotropic material, c can be obtained in terms of the bulk modulus, κ, and the horizon, δ, as

$$c = \frac{18\kappa}{\pi\delta^4} \tag{9}$$

Upon bond, the bond force between pairs of material particles goes to zero, and this can be captured by μ, which is a history-dependent scalar valued function as

$$\mu(t,\xi)=\begin{cases}1 & \text{if } s(t,\xi)<s_0 \quad \text{for all} \quad 0\le t'\le t \\ 0 & \text{otherwise}\end{cases} \tag{10}$$

where s_0 is the critical stretch for bond broken, that will be seen as a constant for the moment. According to Silling and Askari (2005), the critical stretch value can be obtained from the critical energy release rate, G_0, in the case of isotropic materials as

$$s_0=\sqrt{\frac{5G_0}{9\kappa\delta}} \tag{11}$$

As mentioned above, material failure is defined by bond breakage, and one advantage of introducing failure at the bond level is that it introduces a quantity known as local damage at a particle, which can be quantified as

$$\varphi(\boldsymbol{x},t)=\frac{\int_{H_x}\mu(\boldsymbol{x},t,\xi)\mathrm{d}V_\xi}{\int_{H_x}\mathrm{d}V_\xi} \tag{12}$$

In order to carry out the numerical calculation, the region of interest is discretized into uniform sub-domains. A constant displacement and a constant velocity field are then distributed in each sub-domain. The method is meshfree in the sense, because there are no elements or other geometrical connections. Thus, Eq. (1) can be discretized as follows:

$$\rho\ddot{\boldsymbol{u}}_i^n=\sum_j \boldsymbol{f}(\boldsymbol{u}_j^n-\boldsymbol{u}_i^n,\boldsymbol{x}_j-\boldsymbol{x}_i)V_j+\boldsymbol{b}_i^n \tag{13}$$

where k is the time step number and the subscripts denote the material particle number, in which i represents the particle in question and j represents the particles within the horizon of i. V_j is the volume of the material particle j.

The accelerations of each material particle can be calculated by Eq. (13). To acquire displacement of each material particle, second derivative method of the displacements with respect to time is used during proceeding time integration.

NUMERICAL METHOD OF PROPELLER-ICE IMPACT

When an ice-going ship navigates in ice rubble conditions, different shapes and sizes of ice pieces approach the propeller along the bottom of the ship hull. In this process, ice pieces move freely. Due to the interaction among the fluid, ice, and propeller, the ice pieces will impact the propeller blade with random velocities and directions, as shown in Figure 1. Therefore, the process of the propeller-ice impact is very complex.

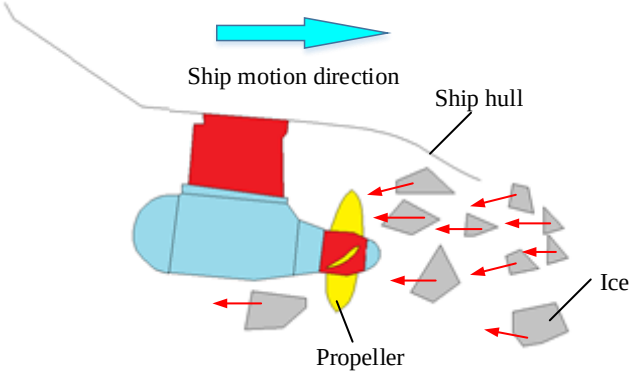

Figure 1. Sketch of propeller-ice impact

For the convenience of research, it is necessary to simplify the propeller-ice impact problem, as shown in Figure 2. The propeller is treated as a rigid body. The shape of the ice piece is usually simplified as a cuboid or sphere. Given that the ice contact force produced by the propeller-ice impact is so dominant, the hydrodynamic forces of the propeller are also neglected.

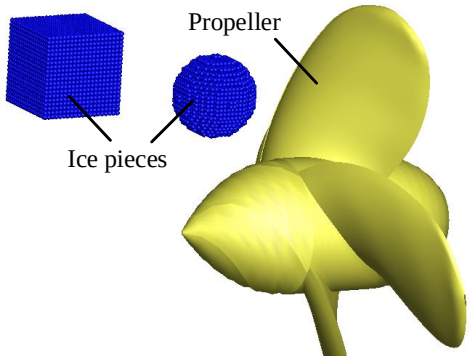

Figure 2. Simplified model of propeller-ice impact problem

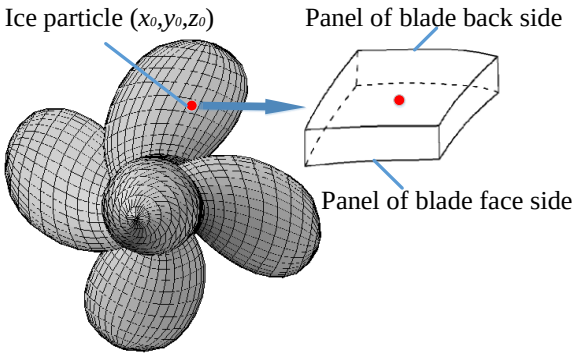

Figure 3. Illustration of the geometrical method to determine the contact ice material particles

To carry out the numerical calculation, the region of interest should be discretized into a number of uniform sub-domains. Ice piece is treated as homogeneous material and discretized by material particles. The surface of a propeller of the propeller blade is divided into a number of small quadrilateral panels along the radial and chordwise directions. Then, the contact detection between propeller blades and ice can be simplified to an easy problem of determining position relationship between ice particles and panel of a propeller blade. A contact detection algorithm has been proposed by Ye et al. (2017) to quickly determine whether the ice particles contact with the propeller. After the possible ice contact particles are identified, further detection of whether the propeller contacts these ice particles can be done by a geometric method. First, two panels corresponding to the back and face sides are located, as shown in Figure 3. Next, the control particles, normal vectors, and plane equations of these two panels can be computed and stored. Last, the location relationship between the particle and the two planes can be discriminated by substituting coordinates of the ice particles into the plane equations.

To calculate ice contact loads, the main attention should be paid to those ice particles that contact the propeller. Once the contact takes place between the propeller and the ice block, there is initially a penetration of ice material particles into the propeller body, as illustrated in Figure 4b. In order to reflect the physical reality, the ice material particles inside the propeller body should be relocated to their new positions outside the propeller surface. Their new locations are assigned to achieve the closest distance to the surface of the propeller, as shown in Figure 4c.

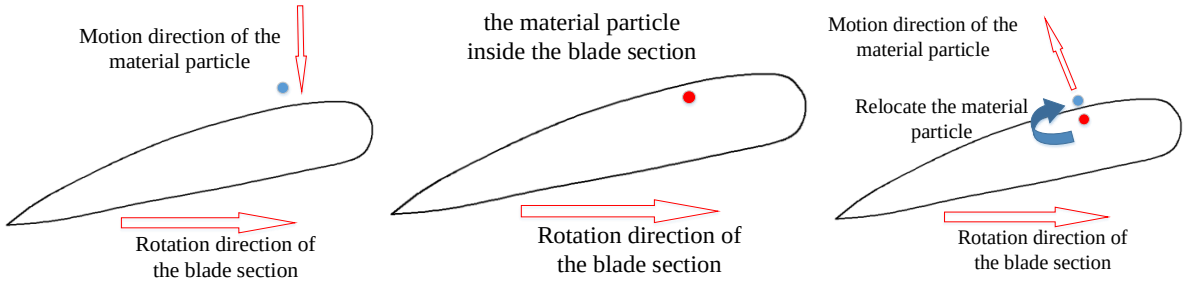

(a) Time, t (b) Time, $t+\Delta t$ (c) Time, $t+\Delta t$ (relocation)

Figure 4. Relocation of material particle inside propeller body: (a) Time, t; (b) Time, $t+\Delta t$; (c) Time, $t+\Delta t$ (relocation)

Based on the location of the ice material particle at t and $t+\Delta t$, one of the two panels of the back and face side can be determined as the panel into which the ice material particle penetrates. Then, the distance between the material particle and the panel is calculated as:

$$d = \frac{\left|A_1 x_0 + B_1 y_0 + C_1 z_0 + D_1\right|}{\sqrt{A_1^2 + B_1^2 + C_1^2}} \tag{14}$$

Its new location can be assigned as:

$$\boldsymbol{x}_{(k)}^{t+\Delta t} = \boldsymbol{x}_{(k)}^{t} + \boldsymbol{V}_0 \cdot \Delta t + d \cdot \boldsymbol{n} \tag{15}$$

Therefore, this process develops a contact surface between the propeller and ice material particles at a particular time, t.

The velocity of such a material particle, $\boldsymbol{x}_{(k)}$, in its new location at the next time step, $t+\Delta t$, can be computed as (Madenci and Oterkus, 2014):

$$\bar{\boldsymbol{v}}_{(k)}^{t+\Delta t} = \frac{\boldsymbol{u}_{(k)}^{t+\Delta t} - \boldsymbol{u}_{(k)}^{t}}{\Delta t} \tag{16}$$

where $\bar{\boldsymbol{u}}_{(k)}^{t+\Delta t}$ is the modified displacement vector at time $t+\Delta t$ and $\boldsymbol{u}_{(k)}^{t}$ represents the displacement vector at time t. At time $t+\Delta t$, the contribution of the material particle, $\boldsymbol{x}_{(k)}$, to the reaction force from the target material to the propeller, $\boldsymbol{F}_{(k)}^{t+\Delta t}$, can be computed from:

$$\boldsymbol{F}_{(k)}^{t+\Delta t} = -1 \times \rho_{(k)} \frac{\bar{\boldsymbol{v}}_{(k)}^{t+\Delta t} - \boldsymbol{v}_{(k)}^{t+\Delta t}}{\Delta t} V_{(k)} \tag{17}$$

where $\boldsymbol{v}_{(k)}^{t+\Delta t}$ is the velocity vector at time $t+\Delta t$ before relocating the material particle $\boldsymbol{x}_{(k)}$, with $\rho_{(k)}$ and $V_{(k)}$ representing its density and volume, respectively. Summation of the contributions of all material particles inside the propeller body results in the forces $\boldsymbol{F}_{(k)}^{t+\Delta t}$ ($F_X^{t+\Delta t}$, $F_y^{t+\Delta t}$, $F_z^{t+\Delta t}$ in the direction of the xyz-axis) and the moments $\boldsymbol{M}^{t+\Delta t}$ ($M_X^{t+\Delta t}$, $M_y^{t+\Delta t}$, $M_z^{t+\Delta t}$ in the direction of the xyz-axis), on the propeller blades at time $t+\Delta t$, and they can be expressed as:

$$\begin{cases} \boldsymbol{F}^{t+\Delta t} = \sum_{k=1} \boldsymbol{F}_{(k)}^{t+\Delta t} \lambda_{(k)}^{t+\Delta t} \\ \boldsymbol{M}^{t+\Delta t} = \sum_{k=1} \boldsymbol{F}_{(k)}^{t+\Delta t} \lambda_{(k)}^{t+\Delta t} \times \boldsymbol{P}_{(k)} \end{cases} \tag{18}$$

where $\boldsymbol{P}_{(k)}$ is the control particle of the panel that contacts the material particle k, and $\lambda_{(k)}^{t+\Delta t}$ can be defined as:

$$\lambda_{(k)}^{t+\Delta t}=\begin{cases}1 & \text{inside impactor}\\ 0 & \text{outside impactor}\end{cases} \tag{19}$$

Thus, the forces, $\boldsymbol{F}_{(k)}^{t+\Delta t}$, and the moments, $\boldsymbol{M}^{t+\Delta t}$, in six degrees of freedom acting on the propeller blade can be calculated.

RESULT AND DISCUSSION

This study uses the Icepropeller1 developed by Ye et al. (2017) as the research model, which is PC3 ice-class. The propeller has a diameter of 4.12m, a blade number of 4, a pitch ratio of 0.76. The ice piece is considered as a sphere or a cuboid located in front of the propeller. The ice spheroid is simplified as a homogeneous material with an elastic modulus of 1.8 GPa, a Poisson's ratio of 0.25, a density of 900 kg/m^3 and a critical stretch of 0.005. Note that, in all the numerical results of the present work, the colors on the ice particles denote the magnitude of the local damage: the color red denotes the largest value and blue denotes the intact.

The Effect of Ice Shape

The dynamic behaviors of propeller impact with ice cuboid and ice sphere are studied. Relative positions between ice and propeller blade are as shown in Figure 5.

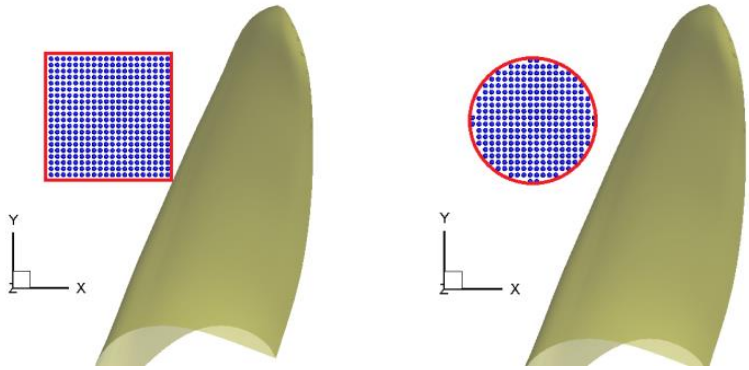

(a) (b)

Figure 5. Relative positon between ice and propeller blade: (a) Ice cuboid; (b) Ice spheroid

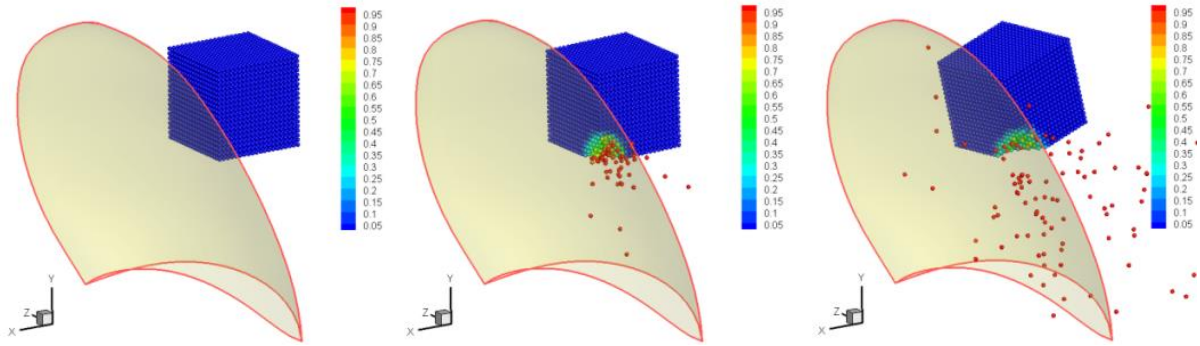

(a) (b) (c)

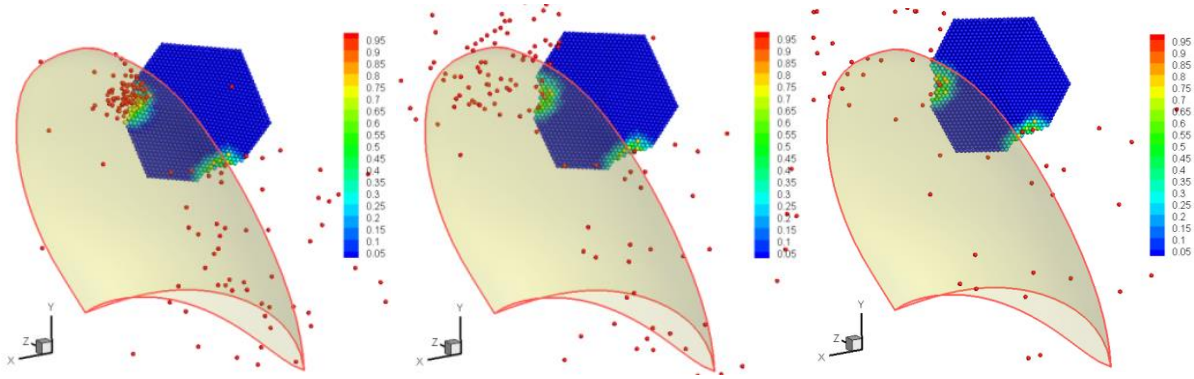

(d) (e) (f)

Figure 6. Dynamic process of propeller impact with ice cuboid: (a) t= 0.0ms; (b) t= 6.96ms; (c) t= 13.92ms; (d) t= 20.88ms; (e) t= 27.84ms; (f) t= 34.8ms

Time series of ice motion and failure is presented in Figure 6. At the moment of t=0.0ms, ice cuboid is in front of the propeller and the impact has not occurred yet, as shown in Figure 6a. With the ice cuboid approaching to the propeller, the nearest end of the ice cuboid will firstly impact on the propeller. Then, the impact position of the ice cuboid will be crushed. As we can see in Figure 6b, the color of the ice material particles changes from blue to red. Since the direction of the impact force does not pass through the center of the ice cuboid, the ice cuboid has an angular acceleration. The ice cuboid will begin to rotate. First impact end of the ice cuboid will depart from the propeller, and the other end of the ice cuboid will approach to the propeller. Then, the second impact between propeller and ice cuboid will occur, as shown in Figure 6d. Due to the impact force, the end of the ice cuboid will depart from the propeller, and the impact will not occur again, as shown in Figures 6e and 6f.

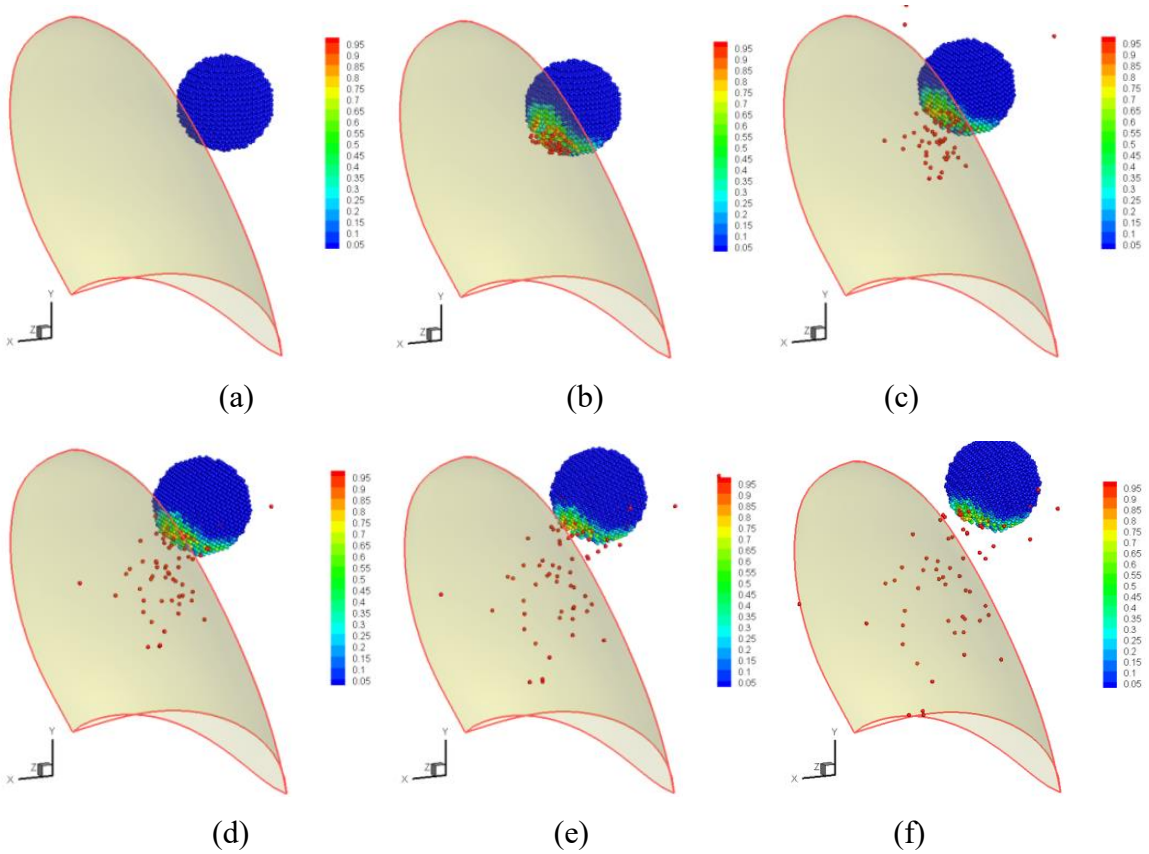

(a) (b) (c)

(d) (e) (f)

Figure 7. Dynamic process of propeller impact with ice sphere: (a) t= 0.0ms; (b) t= 13.92ms; (c) t= 20.88m; (d) t= 27.84ms; (e) t= 34.80ms; (f) t= 41.76ms

Figure 7 shows the time series of ice motion and failure during propeller and ice sphere impact. At the moment of t=0.0ms, ice sphere is in front of the propeller and the impact has not occurred yet, as shown in Figure 7a. With the ice sphere approaching to the propeller, the nearest surface of the ice sphere to the propeller will impact on the propeller. The impact position of the ice sphere will be crushed. From Figure 7b, the color of the ice material particles changes from blue to red. Under the action of impact loads, the whole ice sphere will depart away from the propeller, and the impact will not occur again, as shown in Figure 7e and f. Through the analysis of the impact process, it is found that the impact between propeller and ice sphere occur only once, which is different from that of ice cuboid. It can be explained that since the direction of the impact force does pass through the center of the ice sphere, the ice sphere will not rotate.

Figure 8 shows the time series curves of forces and moments in X-axis direction under ice cuboid and ice sphere impact on the propeller. It is found that the duration time of propeller-ice impact for ice cuboid is longer than that of the ice sphere. It can be explained that ice cuboid is easier to be crushed than ice sphere. In addition, the peak value of ice impact forces and moments for ice cuboid is less than that of the ice sphere.

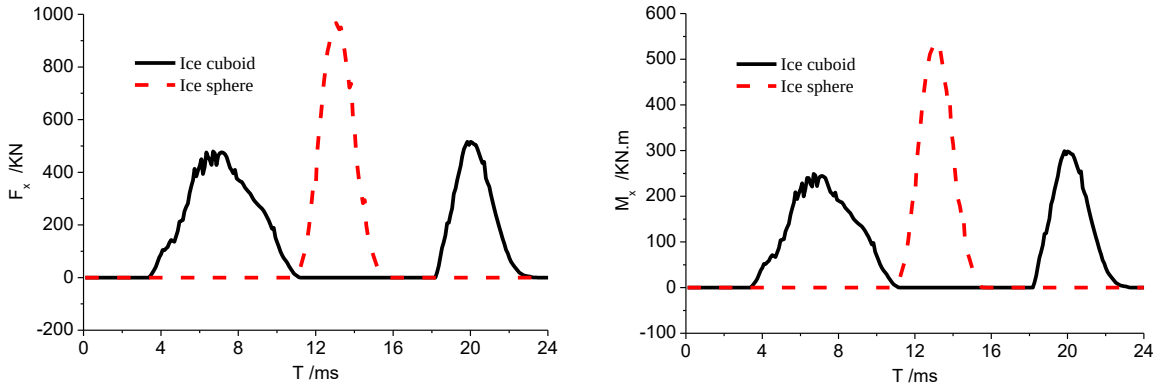

Figure 8. Comparison of ice forces with different ice model: (a) F_x; (b) M_x

The Effect of Ice Velocity

The effects of the ice velocity on the ice failure and dynamic contact load are numerically investigated. The ice model is a spheroid with the diameter d=0.125D. The rotational speed of the propeller is set as 0 rps. Three ice velocities of V_{ice}=10.0 m/s, V_{ice}=20.0 m/s, and V_{ice}=30.0 m/s are tested and the results are discussed.

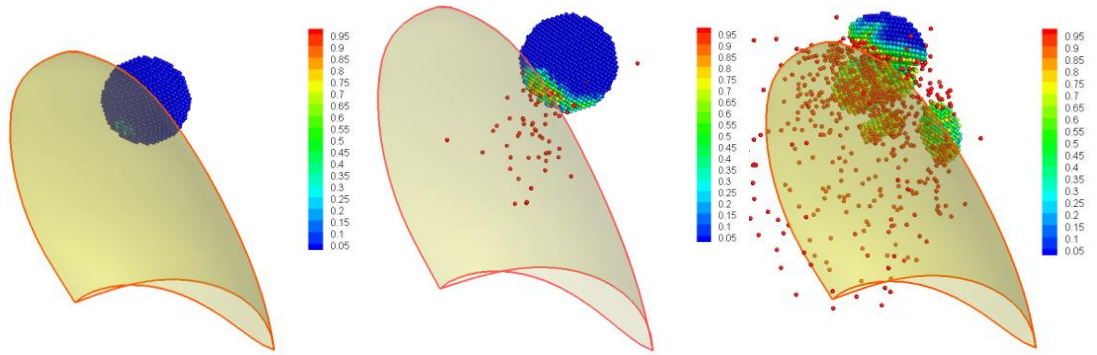

Fig. 9. Ice failure with different ice velocities: (a) 10 m/s;(b) 20 m/s;(c) 30 m/s

The ice failure forms after propeller-ice impact are shown in Fig. 9, from which one may find

that the ice failure degrees are different under different ice velocities. It can be seen that the ice spheroid is slightly damaged for the ice velocity of V_{ice}=10.0 m/s. The damage of the ice spheroid became significant for the ice velocity of V_{ice}=20.0 m/s. However, the ice spheroid is drastically damaged for the ice velocity of V_{ice}=30.0 m/s, which breaks into many ice pieces. It is known from the above analysis that the ice velocity has an effect on the degree of ice failure.

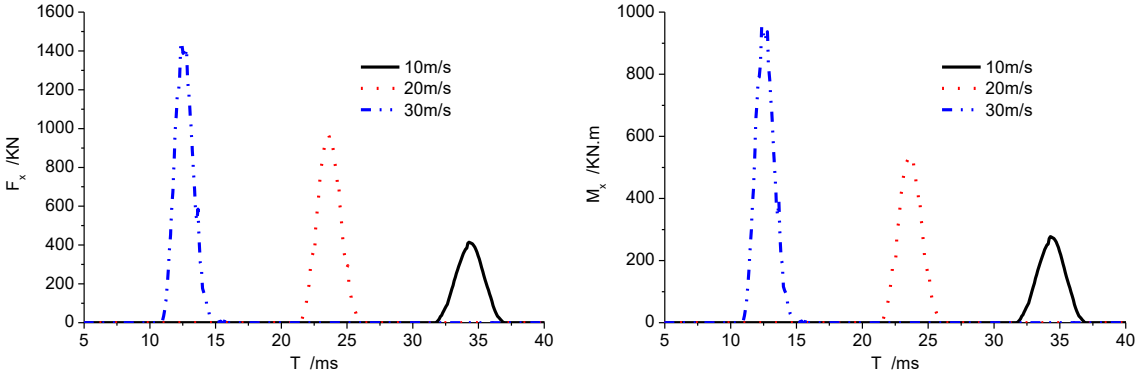

(a) (b)

Fig. 10. Comparison of ice forces with different ice velocities: (a) F_x; (b) M_x

Time histories of ice contact loads with different ice velocities are shown in Fig. 10. The duration during propeller-ice contact can also be found in Fig. 10. It can be seen that the duration with different ice velocities is similar, about 5 ms. However, the peak values of ice contact loads are different. It can be seen from Fig. 10 that the peak force value increases quickly with the increase of ice velocity.

CONCLUSIONS

In this study, a numerical model based on the PD method and the contact detection method is established to study propeller-ice impact. This study addresses the modeling of propeller-ice impact, which is focused on the dynamic characteristics of the ice failure and ice load. Ice cuboid impacts with propeller twice, but Ice sphere impacts with propeller only once, which indicate the shape of ice has a great effect on numerical results. With the increase of ice velocity, the degree of ice failure and the peak value of ice load will quickly increase, but the duration of propeller-ice impact with different ice velocities are similar. The results are helpful to understand the mechanism of propeller-ice impact. In the future, more complicated propeller-ice impact cases may be simulated, such as the interaction between the propeller and multiple ice pieces, to refine the proposed method.

ACKNOWLEDGEMENTS

The research was financially supported by the National Natural Science Foundation of China (Grant NO. 5180905, 5 51679052, 51639004), the Heilongjiang Postdoctoral Fund (Grant NO. LBH-Z18051), the high technology ship of MIIT (Grant NO. 2017-614) and the Defense Industrial Technology Development Program (Grant NO. JCKY2016604B001).

REFERENCES

Brouwer, J., Hagesteijn, G., & Bosman, R., 2013. *Propeller-ice impacts measurements with a six-component blade load sensor*. SMP 2013.

Kannari, P., 1994. *Ice loads on propellers in Baltic conditions* (in Finnish). Helsinki University of Technology, MARC Report D-103

Laskow, V., & Revill, C., 1985. *Study of Strength Requirements for Nozzles for Ice Transiting Ships*: Summary Report (No. TP-6838E).

Lau, M., & Ré, A. S., 2010. Performance of survival craft in ice environments.

Madenci, E., & Oterkus, E., 2014. *Peridynamic theory and its applications* (Vol. 17). New York: Springer.

Shen, H. T., Su, J., & Liu, L. (2000). Sph simulation of river ice dynamics. *Journal of Computational Physics*, 165(2), 752-770.

Silling, S. A., 2000. Reformulation of elasticity theory for discontinuities and long-range forces. *Journal of the Mechanics and Physics of Solids*, 48(1), 175-209.

Silling, S. A., Askari, E., 2005. A meshfree method based on the peridynamic model of solid mechanics. *Computers & structures*, 83(17), 1526-1535.

Wang, C., Xiong, W. P., Chang, X., Ye, L. Y., & Li, X. (2018). Analysis of variable working conditions for propeller-ice interaction. *Ocean Engineering*, 156, 277-293.

Wind, J., 1984. The dimensioning of high power propeller systems for arctic ice breakers and icebreaking vessels. *International shipbuilding progress*, 31(357), 131-148.

Ye, L. Y., Wang, C., Chang, X., et al, 2017. Propeller-ice contact modeling with peridynamics. *Ocean Engineering*, 139, 54-64.